13th International Symposium on Turbulence and Shear Flow Phenomena (TSFP13)
Montreal, Canada, June 25-28, 2024

Direct numerical simulation of turbulent channel flow with opposition control based on nonlinear forecasting

Togo Terui, Hiroya Mamori*, Takeshi Miyazaki
Department of Mechanical and Intelligent Systems Engineering
The University of Electro-Communications
1-5-1 Chofugaoka, Chofu, Tokyo, 182-8585, Japan
*mamori@uec.ac.jp

Yusuke Nabae, Hiroshi Gotoda
Department of Mechanical Engineering
Tokyo University of Science
6-3-1 Niijuku, Katsushika-ku, Tokyo, 125-8585, Japan

ABSTRACT
Skin-friction drag reduction of wall turbulence is essential to reduce an environmental impact. It is well-known that the feedback control technique provides the drag reduction effect with a significant gain. In this study, we employ an opposition control technique: blowing and suction are applied to the wall to cancel out turbulent vortical structures in the region near the wall. The detected velocity is immediately used as the control input in the ordinary opposition control. However, in the present study, the near-wall velocity is predicted by the orbital-instability-based forecasting method based on the deterministic chaos of the low-Reynolds−number flow. We perform direct numerical simulations of turbulent channel flows. The drag reduction rate is comparable to that of the ordinary opposition control.

INTRODUCTION
Many control techniques are examined to decrease the skin friction drag in wall turbulence. Controlling skin-friction drag in turbulent flows is essential to mitigating the environmental impact. The opposition control performed by Choi et al. (1994) is a well-known feedback control: the wall-normal blowing and suction are added to cancel out the near-wall velocity detecting on the sensing plane. The skin-friction drag reduction rate is 25% at $\mathrm{Re}_\tau = 180$, and the detection surface height of $y_d^+ = 15$. When the skin-friction drag is reduced, a virtual wall is formed between the detecting plane and the wall surface (Hammond et al., 1998; Chung and Talha, 2011).

Nonlinear time series analysis, inspired by dynamical systems theory, has succeeded in extracting the deterministic chaos in irregularly fluctuating physical quantities by focusing on two essential properties: fractals as self-similar structures and short-term predictability and long-term unpredictability associated with the strong sensitivity of initial condition (e.g., Holger and Thomas, 2003). Mamori et al. (2023) have reported that the nonlinear analysis enables the prediction of the complex flow field to be predicted even in wall turbulence.

In this study, we investigate the application of time series prediction of the wall-normal velocity to the opposition control. This attempt corresponds to considering the time delay of the opposition control. The opposition control is one of the feedback control techniques, and a time delay occurs between the detection of velocity at the sensing and the control input.

DIRECT NUMERICAL SIMULATION
We performed the direct numerical simulation of the fully developed and incompressible turbulent channel flow. The mean pressure gradient in the streamwise direction is kept constant. The reference length and velocity are the channel half-width δ^* and the friction velocity u_τ^*, respectively. The asterisk means dimensional variables. The governing equations are the continuity and Navier-Stokes equations.

$$\frac{\partial u_i}{\partial x_i} = 0 \tag{1}$$

$$\frac{\partial u_i}{\partial t} + \frac{\partial u_j u_i}{\partial x_j} = -\frac{\partial p}{\partial x_i} + \frac{1}{\mathrm{Re}_\tau}\frac{\partial^2 u_i}{\partial x_j \partial x_j} \tag{2}$$

The streamwise, wall-normal, spanwise coordinates and the corresponding velocity components are denoted as (x, y, z) and (u, v, w), respectively. In addition, t is time, and p is the pressure. All the simulations start from the fully developed and turbulent flow, and the control begins at $t = 0$. As time advances, we employ the second-order Crank-Nicolson method for the viscous term and the low-storage third-order Runge-Kutta method for the other terms. The friction Reynolds number is set to be Re_τ (= $u_\tau^* \delta^* / \nu^*$) = 180, which corresponds to the bulk Reynolds number of Re_b (= $2u_b^* \delta^* / \nu^*$) = 5600 in the uncontrolled flow. Here, u_b^* and ν^* are the bulk velocity and the kinematic viscosity, respectively.

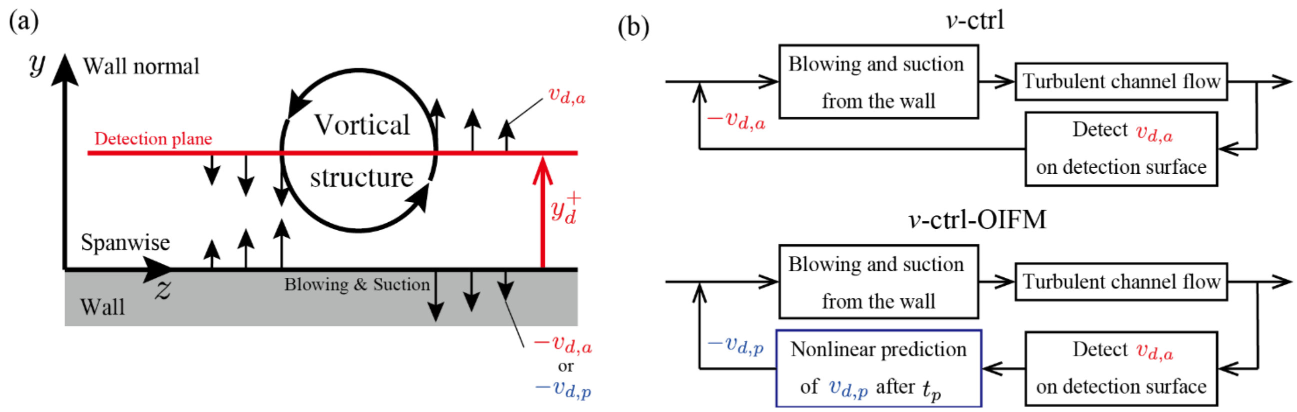

Figure 1. (a) Schematic and (b) diagram of the opposition control.

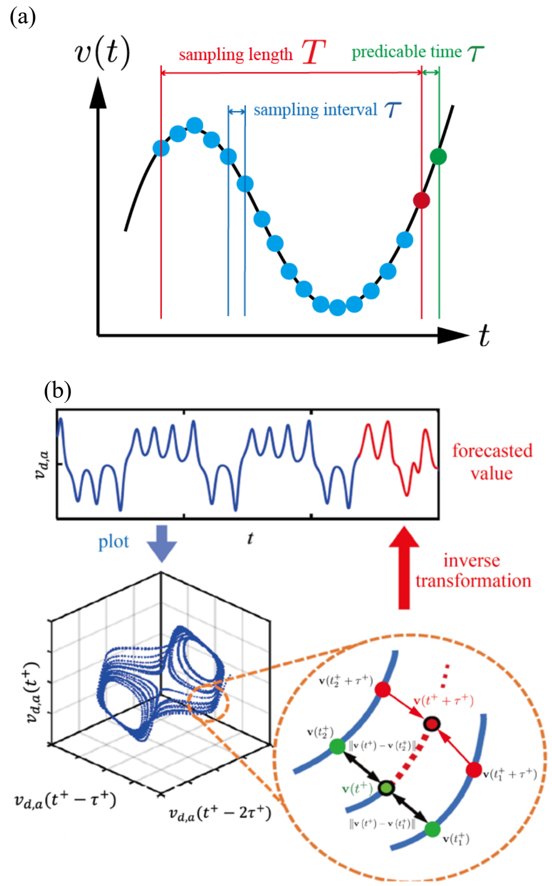

Figure 2. (a) Definition of the sampling time and (b) the orbital-instability-based forecasting method.

The computational domain is $(L_x, L_y, L_z) = (2\pi, 2, \pi)$ and grid points are $(N_x, N_y, N_z) = (256, 96, 128)$. We employ a staggered grid system: grid size is uniform in the homogeneous directions and nonuniform in the wall-normal direction. The periodic boundary conditions are imposed in the streamwise and spanwise directions, and the no-slip condition is imposed on the wall.

Figure 1 shows the schematic of the opposition control. In an ordinary opposition control (Choi et al., 1994), the blowing and suction are applied on the wall to cancel out the vortical structure (referred to as "v-ctrl"). The control input is the opposite sign of the wall-normal velocity on the detection plane, and the time delay is not considered. We examine the opposition control with the orbital-instability-based forecasting method ("v-ctrl-OIFM"). The orbital-instability-based forecasting method is proposed by Gotoda et al. (2015).

Figure 2 shows the schematic of the nonlinear forecasting method. As shown in Fig. 2(a), we predict the velocity $v(t+\tau)$ from the library data. Here, T and τ denote the sampling length and the constant sampling interval. The wall-normal velocity on the detection surface $v_{d,a}$ is stored in a library. Figure 2(b) shows the orbital-instability-based forecasting method (the OIFM, hereafter). The D_e-dimensional space of $\mathbf{v}(t_i)=(v_{d,a}(t_i), v_{d,a}(t_i-\tau), \ldots, v_{d,a}(t_i-\tau(D_e-1)))$ is extracted from the library data, and the trajectory is drawn. If the sampling data is the deterministic chaos, the trajectory is the "attractor." Therefore, we can forecast $\boldsymbol{v}(t+\tau)$ from the neighborhood trajectories. Specifically, the forecasted velocity is obtained from the velocity data.

$$\mathbf{v}(t+\tau) = \frac{\sum_{k=1}^{K} \mathbf{v}(t_k+\tau) \exp(-\|\mathbf{v}(t) - \mathbf{v}(t_k)\|)}{\sum_{k=1}^{K} \exp(-\|\mathbf{v}(t) - \mathbf{v}(t_k)\|)} \tag{3}$$

$$v_{d,p} = v_{d,a}(t+\tau) \tag{4}$$

Here, τ is the predicted time, and K is the number of nearby points. In this study, we investigate the effect of T and τ in $360 \le T^+ \le 2880$, $0.18 \le \tau^+ \le 1.44$. Other parameters are fixed at $y_d^+ = 16$, $\Delta t^+ = 0.036$, $D_e = 5$ and $K = 50$. The superscript of the plus denotes the wall unit, i.e., non-dimensionalized by u_τ^* and ν^*.

RESULTS AND DISCUSSION

Figure 3 shows the drag reduction ratio R_D.

$$R_D = \frac{C_{f,0} - C_f}{C_{f,0}} \times 100 \tag{4}$$

Here, C_f is the wall friction coefficient, and zero subscript indicates the uncontrolled case. The time-averaged value at the fully developed state is used. The R_D of v-ctrl is 24.8%. In the

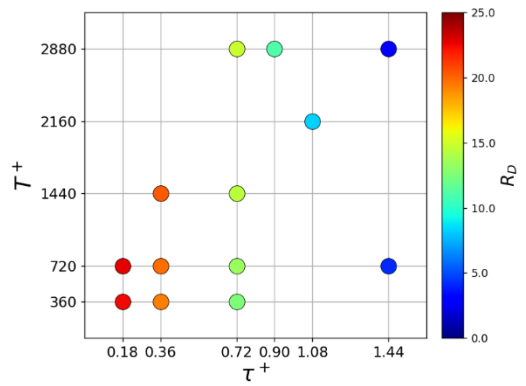

Figure 3. R_D values of each case.

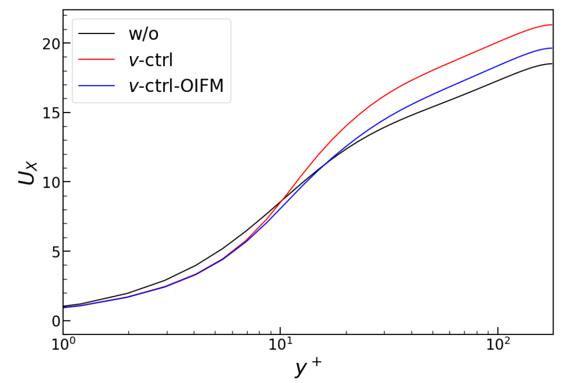

Figure 7. Streamwise velocity.

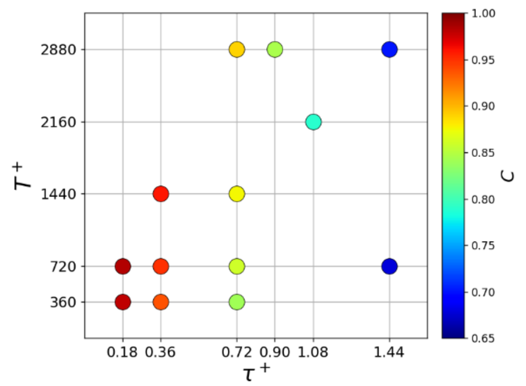

Figure 4. C values of each case.

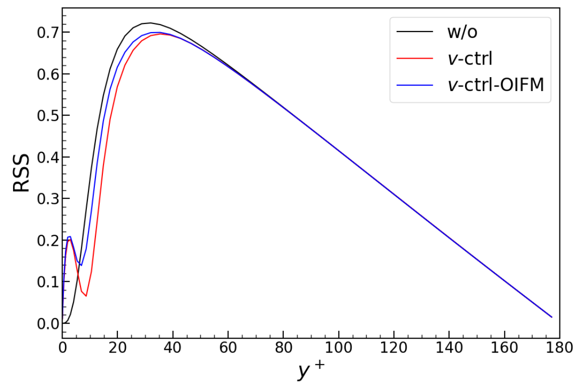

Figure 8. Reynolds Shear Stress (RSS).

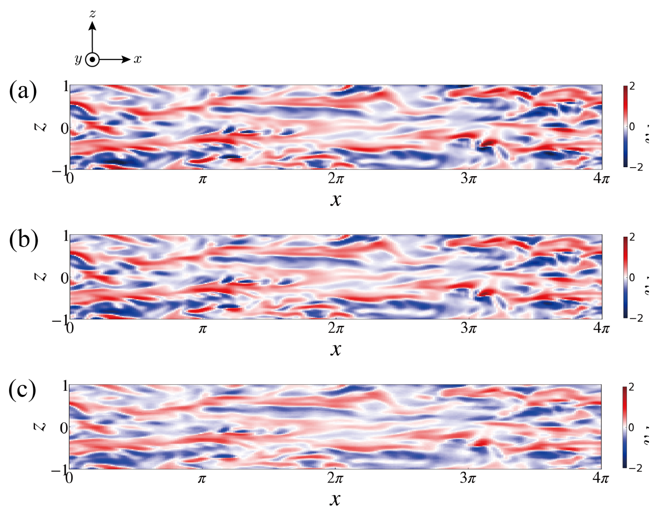

Figure 5. Instantaneous distribution of (a) $v_{d,a}$ and (b) $v_{d,p}$ of (τ^+, T^+) = (0.36, 720) and (c) (τ^+, T^+) = (1.44, 720) on the detection plane at t=0.

cases of v-ctrl-OIFM, R_D increases for the smaller τ^+ and the larger T^+. However, the effect of τ^+ is considerably more significant than that of T^+. In the case of (τ^+, T^+) = (0.18, 720), we obtain R_D = 22.8%, close to the v-ctrl.

Figure 4 shows the correlation coefficient C between the predicted and the actual velocities, $v_{d,p}$ and $v_{d,a}$.

$$C = \frac{Corr[v_{d,a}(t),\ v_{d,p}(t)]}{v_{d,a}(t)_{\mathrm{rms}} v_{d,p}(t)_{\mathrm{rms}}} \tag{5}$$

The trend of C is similar to that of R_D. Although smaller τ^+ will provide a more significant drag reduction effect, for practical use, τ^+ must have a specific value in terms of the time resolution of the velocity sensor. Therefore, we chose parameter sets of (τ^+, T^+) = (0.72, 720) as a reference case of v-ctrl-OIFM. The predictable time τ^+ is 20 times Δt^+. The R_D and C of that case are 13.5% and 0.86, respectively. Iwamoto et al. (2004) also showed that the v-ctrl gives the drag reduction effects at high-Reynolds number flows. Therefore, it is expected that v-ctrl-OIFM also has a drag reduction effect even at high-Reynolds number flows.

Figure 5 compares the instantaneous distributions of the predicted velocity $v_{d,p}$ in two different cases of (τ^+, T^+) = (0.36, 720) and (1.44, 720) and the actual velocity $v_{d,a}$ at t = 0. The correlation in the v-ctrl-OIFM case of (τ^+, T^+) = (0.36, 720) is C = 0.95 and another v-ctrl-OIFM case is C = 0.68. While the velocity distributions are almost predicted, the large fluctuation is not predicted (colored by the dark blue and red). The large fluctuation can be reasonably predicted in the former case, in which the correlation coefficient is C = 0.95.

Figure 6 shows the streamwise velocity of the uncontrolled case, v-ctrl, and v-ctrl-OIFM. The mean velocities of the v-ctrl and v-ctrl-OIFM are larger than those of the uncontrolled case in the center of the channel. This corresponds to a large drag reduction because the present simulation is made under the constant pressure gradient condition.

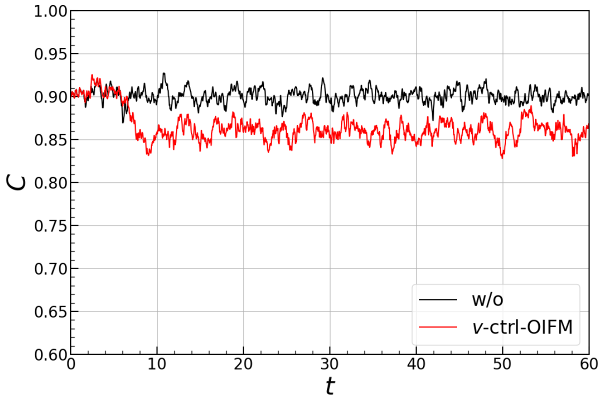

Figure 9. Time trace of C values.

Figure 8 compares the RSS of the uncontrolled case, v-ctrl, and v-ctrl-OIFM. The virtual wall is formed between the wall and the detection surface (at y^+=8), where the RSS is significantly decreased for controlled cases. However, the RSS of v-ctrl-OIFM is more significant than that of v-ctrl, which corresponds to the large fluctuation that is not accurately predicted.

Figure 9 shows the time trace of C of the uncontrolled and reference cases. The time-averaged value of C in the uncontrolled case is 0.90, and that of the reference case is 0.86. The control input slightly changes the chaotic trajectory in the phase space while the library is updated sequentially.

SUMMARY

Direct numerical simulation of the turbulent channel flow with the opposition control is performed. The near-wall velocity is predicted by the orbital-instability-based forecasting method. The drag reduction rate R_D by the present methods is 22.8%, comparable with the ordinary opposition control (R_D = 24.8%). The library, especially the sampling interval τ, affects the drag reduction rate R_D: the smaller τ leads to a large R_D. The dependence is similar to the correlation coefficient C between the predicted and actual velocities. The predicted velocity is almost similar to the actual velocity, while the large fluctuation is not predicted accurately. The virtual wall is formed between the wall and the detection surface, while the decrease in the RSS is insufficient compared to the ordinary opposition control case.

REFERENCES

Choi, H., Moin, P., and Kim, J., 1994, “Active turbulence control for drag reduction in wall-bounded flows”, *Journal of Fluid Mechanics*, 262, 75-110.

Chung, Y. M. and Talha, T., 2011, “Effectiveness of active flow control for turbulent skin friction drag reduction”, *Physics of Fluids*, 23, 025102.

Gotoda, H., Okuno, Y., and Tachibana, S., 2015, “Characterization of degeneration process in combustion instability based on dynamical systems theory”, *Physical Review E* 92, 052906.

Hammond, E. P., Bewley, T. R., and Moin, P., 1998, “Observed mechanisms for turbulence attenuation and enhancement in opposition-controlled wall-bounded flows”, *Physics of Fluids*, 10, 2421-2423.

Holger, H and Thomas, S., 2003, " Nonlinear Time Series Analysis", 2nd ed., *Cambridge University Press*.

Iwamoto, K., Fukagata, K., Kasagi, N., and Suzuki, Y., 2004, “DNS of turbulent channel flow at Re_τ = 1160 and evaluation of feedback control at practical Reynolds numbers.”, *Proceeding of 5th International Symposium on Smart Control of Turbulence*.

Mamori, H., Nabae, Y., Fukuda, S., and Gotoda, H., 2023, “Dynamic state of low-Reynolds-number turbulent channel flow”, *Physical Review E* 108, 025105.

Small, M., 2005, “Applied nonlinear time series analysis: applications in Physics, Physiology and Finance”, *World Scientific Series on Nonlinear Science Series A* 52.